

Lagrangian ocean analysis

Erik Van-Sebille et al.



Lagrangian ocean analysis: Fundamentals and practices



Erik van Sebille^{*,a,b}, Stephen M. Griffies^c, Ryan Abernathey^d, Thomas P. Adams^e, Pavel Berloff^f, Arne Biastoch^g, Bruno Blanke^h, Eric P. Chassignetⁱ, Yu Cheng^j, Colin J. Cotter^f, Eric Deleersnijder^{k,l}, Kristofer Döösⁿ, Henri F. Drake^{o,p}, Sybren Drijfhout^q, Stefan F. Gary^e, Arnold W. Heemink^l, Joakim Kjellsson^{r,t}, Inga Monika Koszalka^{g,aa}, Michael Lange^{a,s}, Camille Lique^h, Graeme A. MacGilchrist^u, Robert Marsh^q, C. Gabriela Mayorga Adame^v, Ronan McAdam^a, Francesco Nencioli^w, Claire B. Paris^j, Matthew D. Piggott^s, Jeff A. Polton^v, Siren Rühls^g, Syed H.A.M. Shah^{m,1}, Matthew D. Thomas^x, Jinbo Wang^y, Phillip J. Wolfram^z, Laure Zanna^t, Jan D. Zika^{a,bb}

^a *Grantham Institute & Department of Physics, Imperial College London, UK*

^b *Institute for Marine and Atmospheric Research, Utrecht University, Utrecht, Netherlands*

^c *NOAA / Geophysical Fluid Dynamics Laboratory, Princeton, USA*

^d *Department of Earth and Environmental Sciences, Columbia University, NY, USA*

^e *Scottish Association for Marine Science, Oban, UK*

^f *Department of Mathematics, Imperial College London, UK*

^g *GEOMAR Helmholtz Centre for Ocean Research Kiel, Kiel, Germany*

^h *Laboratoire d'Océanographie Physique et Spatiale, UMR 6523, CNRS-IFREMER-IRD-UBO, Brest, France*

ⁱ *Center for Ocean-Atmospheric Prediction Studies, Florida State University, Tallahassee, FL, USA*

^j *Department of Ocean Sciences, Rosenstiel School of Marine and Atmospheric Science, University of Miami, USA*

^k *Université catholique de Louvain, Institute of Mechanics, Materials and Civil Engineering (IMMC) & Earth and Life Institute (ELI), Louvain-la-Neuve, Belgium*

^l *Delft Institute of Applied Mathematics (DIAM), Delft University of Technology, Netherlands*

^m *Department of Mathematics, Sukkur Institute of Business Administration, Pakistan*

ⁿ *Department of Meteorology, Bolin Centre for Climate Research, Stockholm University, Sweden*

^o *Department Atmospheric and Oceanic Sciences, Princeton University, USA*

^p *Currently at Massachusetts Institute of Technology and Woods Hole Oceanographic Institution Joint Program in Oceanography, USA*

^q *University of Southampton, UK*

^r *British Antarctic Survey, Cambridge, UK*

^s *Department of Earth Science and Engineering, Imperial College London, UK*

^t *Department of Physics, University of Oxford, UK*

^u *Department of Earth Sciences, University of Oxford, UK*

^v *National Oceanography Centre, Liverpool, UK*

^w *Remote Sensing Group, Plymouth Marine Laboratory, Plymouth, UK*

^x *School of Geology and Geophysics, Yale University, USA*

^y *Jet Propulsion Laboratory, California Institute of Technology, USA*

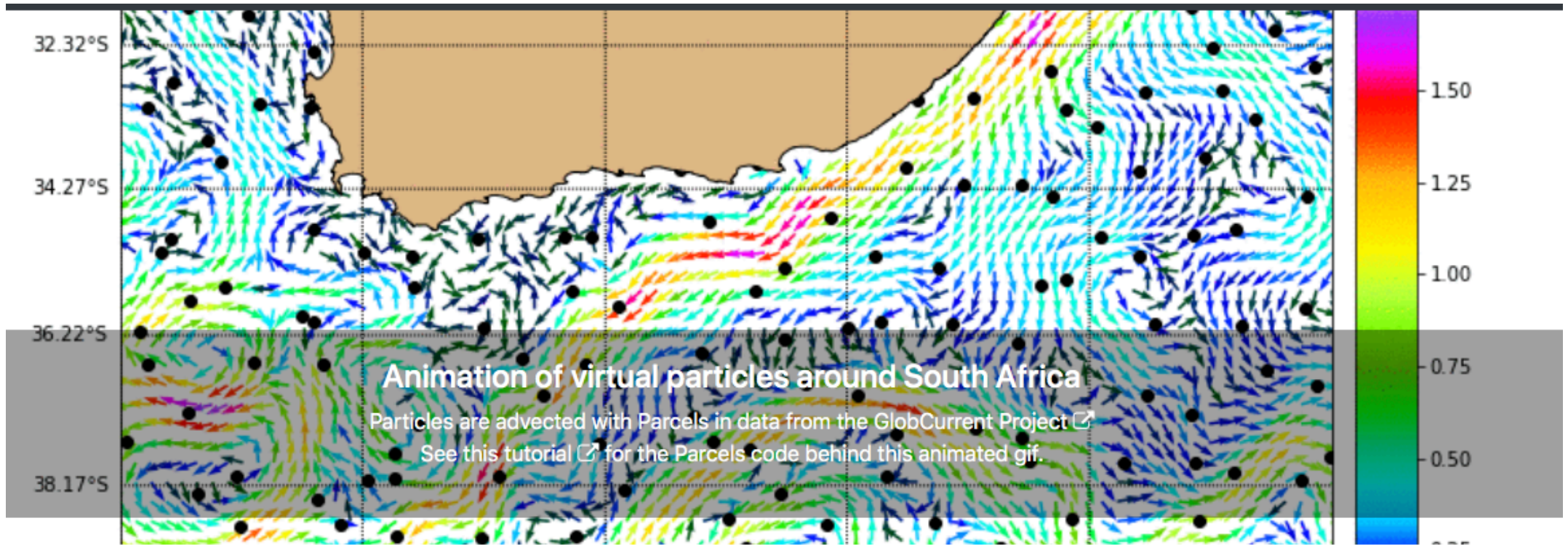
^z *Climate, Ocean and Sea Ice Modeling, Theoretical Division: Fluid Dynamics and Solid Mechanics, Los Alamos National Laboratory, Los Alamos, NM, USA*

^{aa} *Christian-Albrechts University of Kiel, Kiel, Germany*

^{bb} *School of Mathematics and Statistics, University of New South Wales, Sydney, Australia*

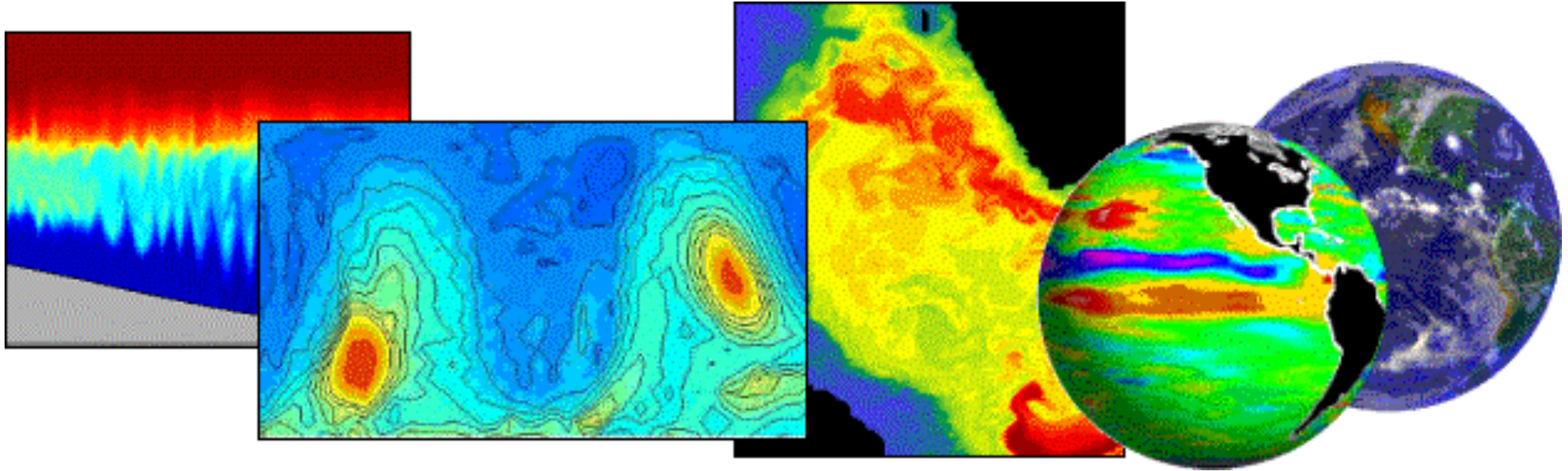
Outline:

- Motivation
- Fokker-Planck Tracer Equation
- Stochastic Trajectories
- Particle Diagnostics
- Markov Matrices

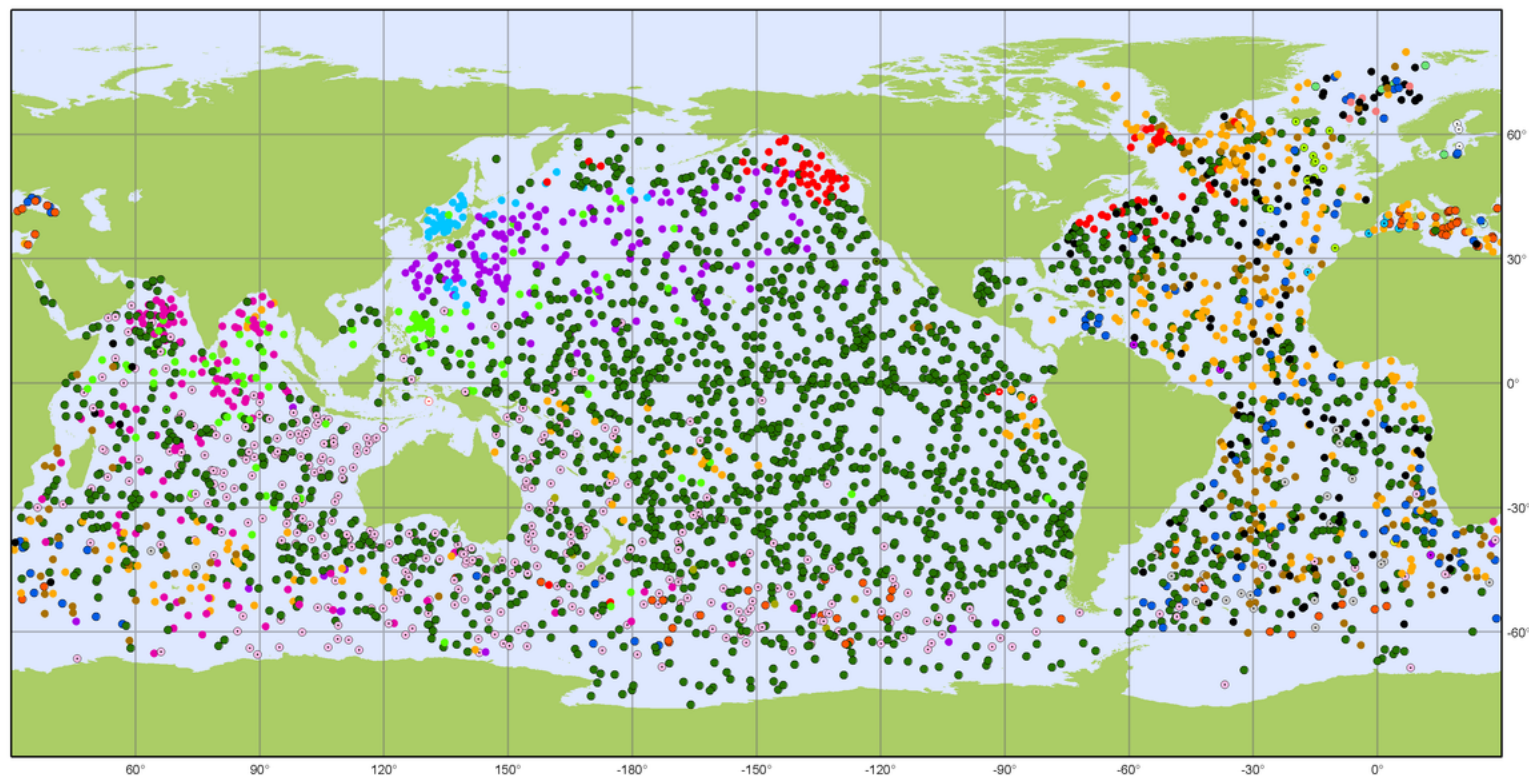


Source: oceanparcels.org

“Trajectories for virtual particles map out pathlines of the velocity field, often including the effect of subgrid scale diffusion. Statistics of the trajectories then define particle pathways and their associated time scales. By following the flow of virtual particles, and possibly assigning non-zero transports and other properties to them in post-processing, questions about pathways and flow connectivity can be addressed.”



Source: nasa.gov



Argo

National contributions - 3881 Operational Floats

February 2018

Latest location of operational floats (data distributed within the last 30 days)

- | | | | | | |
|-------------------|-----------------|-----------------|--------------------|---------------------------|--------------|
| ● ARGENTINA (1) | ● EUROPE (94) | ● INDIA (124) | ● KENYA (1) | ● PERU (3) | ● USA (2179) |
| ○ AUSTRALIA (361) | ○ FINLAND (3) | ○ INDONESIA (1) | ● MEXICO (2) | ● POLAND (5) | |
| ● BRAZIL (3) | ● FRANCE (277) | ● IRELAND (12) | ○ NETHERLANDS (24) | ● KOREA, REPUBLIC OF (53) | |
| ● CANADA (87) | ● GERMANY (142) | ● ITALY (65) | ● NEW ZEALAND (6) | ● SPAIN (5) | |
| ● CHINA (105) | ○ GREECE (2) | ● JAPAN (156) | ● NORWAY (7) | ● UK (163) | |



Generated by www.jcommops.org, 02/03/2018

Source: research.noaa.gov



Amy Bower and a technician with a RAFOF float. Credit: Tom Kleindinst, © Woods Hole Oceanographic Institution

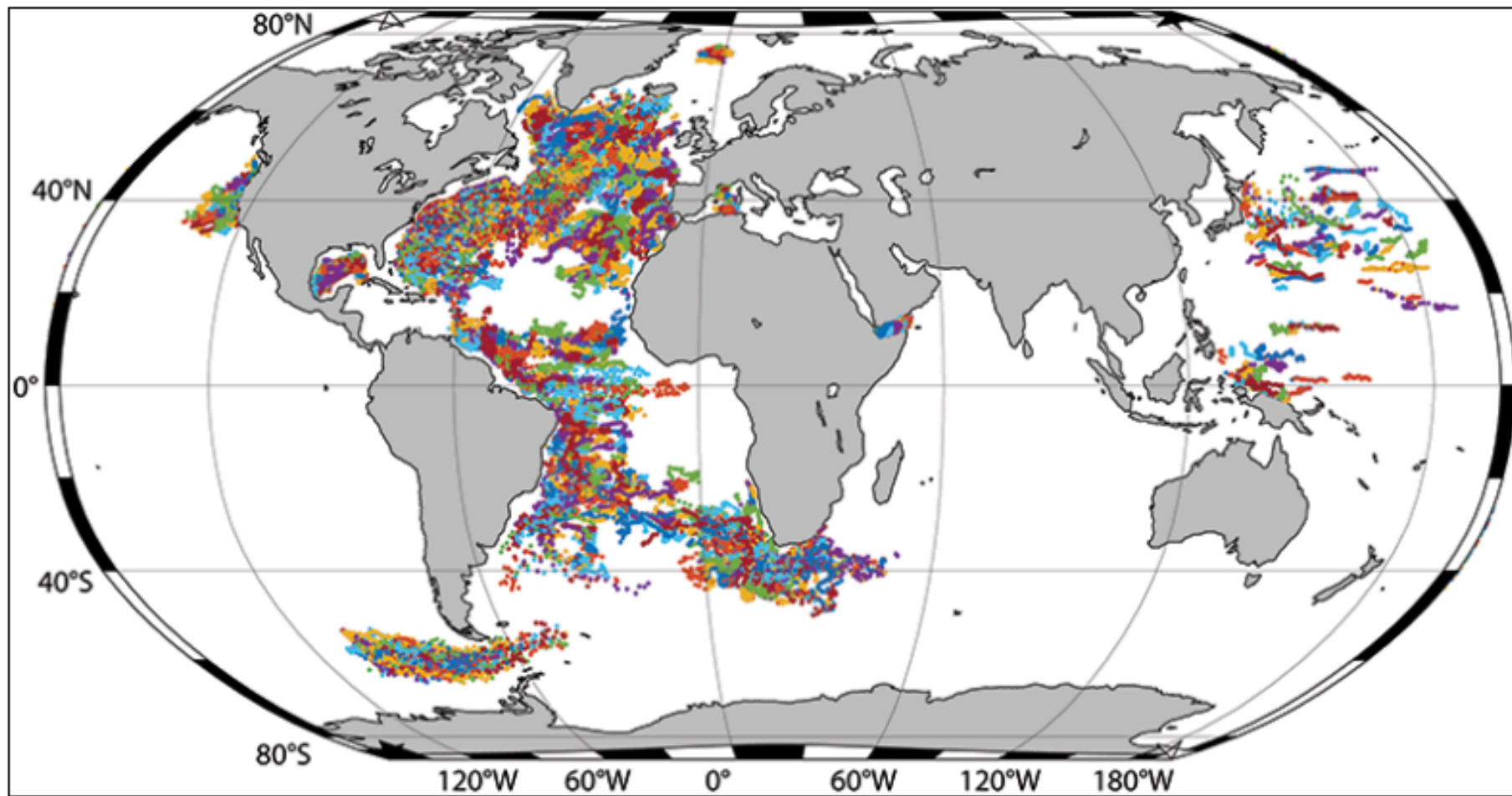
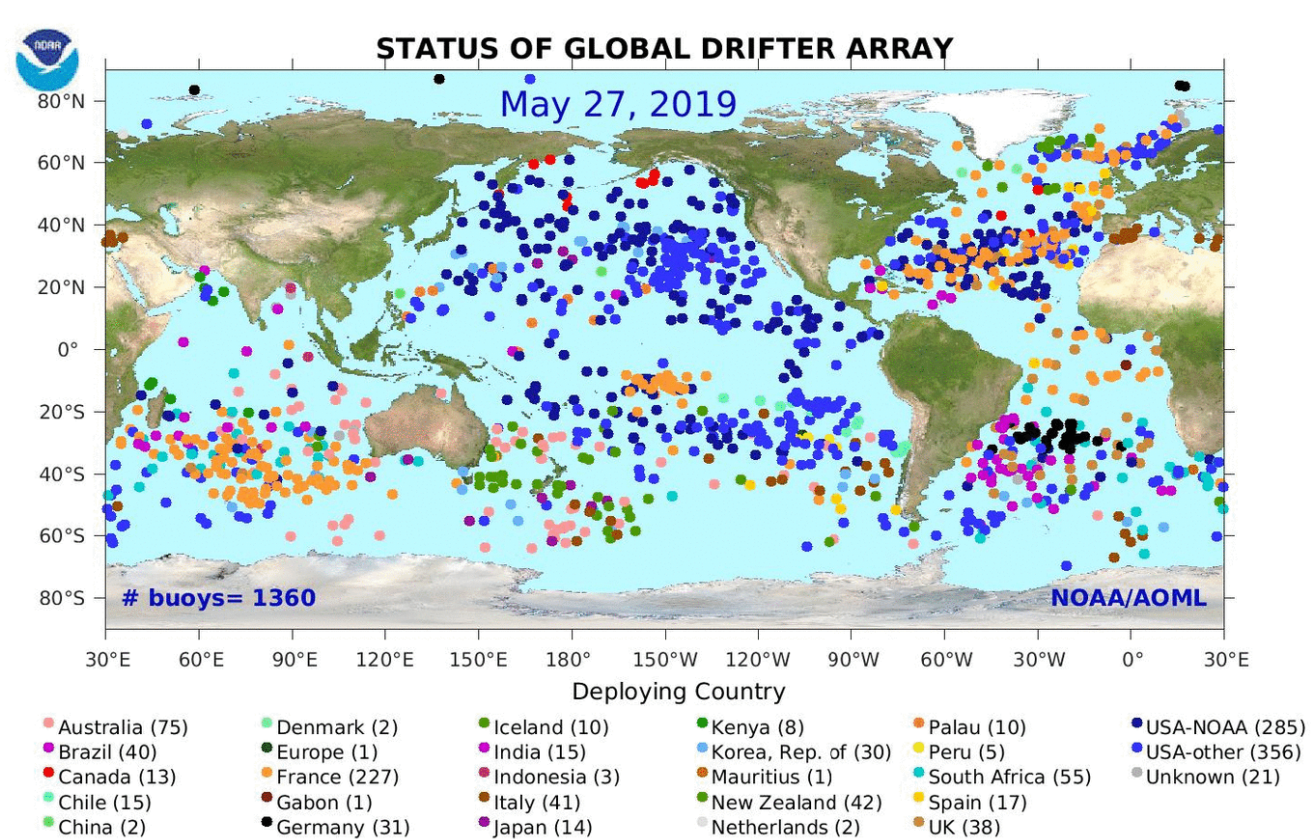


Fig. 3. All acoustically tracked float trajectories in the AOML database as of May 2018. Colors are used to visually distinguish different float tracks.



Source: hawaii.edu

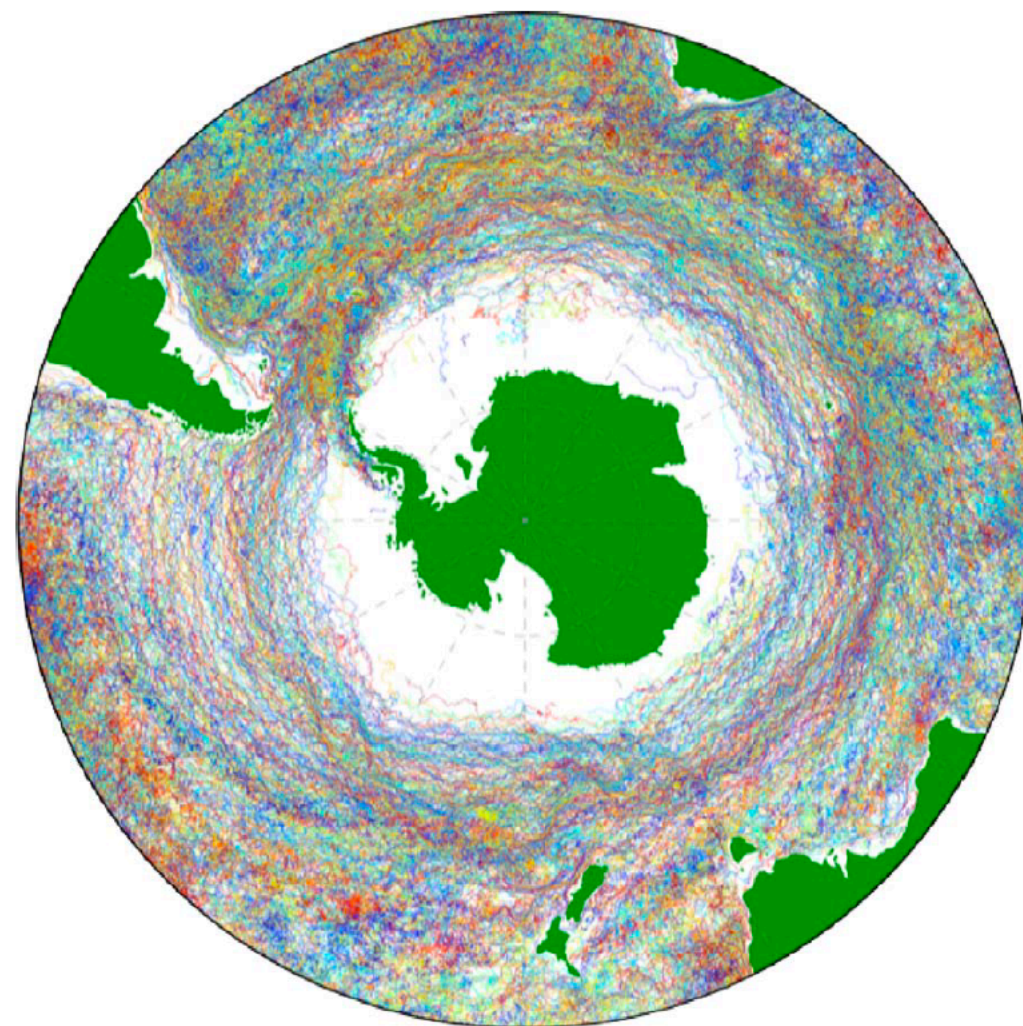



Fig. 1. Map of all the Southern Ocean observational Lagrangian surface drifters in the NOAA GDP Data Set (Lumpkin and Pazos, 2007). Each drifter is geo-located every 6 h and has a randomly assigned colour. (For interpretation of the references to colour in this figure legend, the reader is referred to the web version of this article.)

2.5.1 Tracer Equation with subgrid scale transport

C = Concentration

$$\left(\frac{\partial}{\partial t} + \mathbf{v} \circ \nabla \right) C = \nabla \circ (\mathbf{J} \circ \nabla C)$$

Transport
tensor



$$\mathbf{J} = \mathbf{K} + \mathbf{A}$$

Symmetric
component

Antisymmetric
Component

2.5.1 Tracer Equation with subgrid scale transport

C = Concentration

$$\left(\frac{\partial}{\partial t} + \mathbf{v} \circ \nabla\right)C = \nabla \circ (\mathbf{J} \circ \nabla C)$$

Transport
tensor

$$\mathbf{J} = \mathbf{K} + \mathbf{A}$$

Symmetric
component

Antisymmetric
Component

$$\left(\frac{\partial}{\partial t} + \mathbf{v}^\dagger \circ \nabla\right)C = \nabla \circ (\mathbf{K} \circ \nabla C)$$

$$\mathbf{v}^\dagger = \mathbf{v} + \mathbf{v}^* \quad \text{Residual mean velocity}$$

$$v_j^* = -\partial_i A_{ij} \quad \text{Eddy induced velocity}$$

By definition of \mathbf{A} , \mathbf{v}^* is divergence free, and we can write the tracer equation in the flux form

$$\frac{\partial C}{\partial t} + \nabla \circ (\mathbf{v}^\dagger C) = \nabla \circ (K \circ \nabla C)$$

Apply chain rule identity to get into Fokker-Planck form

$$\frac{\partial C}{\partial t} + \nabla \circ (\mathbf{v}^{drift} C) = \partial_{ij} (K_{ij} C)$$

$$\mathbf{v}^{drift} = v^\dagger + \nabla \circ K$$

$$\nabla \circ \mathbf{v}^{drift} = \partial_{ij} K_{ij}$$

Does not generally vanish which implies
tracer streamtubes are not generally
useful

“For volume transport pathways, one needs a non-divergent velocity field. A three-dimensional non-divergent velocity can be produced by sampling a Boussinesq ocean model, thus offering a means to compute three-dimensional trajectories. To compute tracer transport trajectories, we need both a velocity field and a diffusion tensor. The diffusion tensor is a function of the often poorly known subgrid scale flow, and it is generally a complex function of the flow field. Consequently, the calculation of tracer transport pathways is somewhat less mature than volume transport pathways”

“As an alternative to velocities generated by OGCMs, we may use observation-based data from floats or drifters, which generally give a two dimensional surface velocity (e.g., Koszalka et al., 2011). We may also diagnose a surface geostrophic velocity by differentiating gridded satellite observations of the sea surface height (e.g., Klocker et al., 2012b). Notably, both surface drifter/float velocities and surface geostrophic velocities generally have a non-zero horizontal divergence (surface geostrophic velocities are non-divergent only on an f-plane), and the corresponding surface trajectories do therefore not map volume transport pathways. Nonetheless, the resulting surface trajectories do map preferred pathways of the surface flow, thus providing useful diagnostic information.”

What is the best way to validate these Lagrangian estimates?

3.2 Explicit Virtual Particle Trajectories

Many interpolation schemes and particle tracking schemes referenced in the paper. Several have been discussed in the seminar series. This figure is displayed to encourage discussion on the topic.

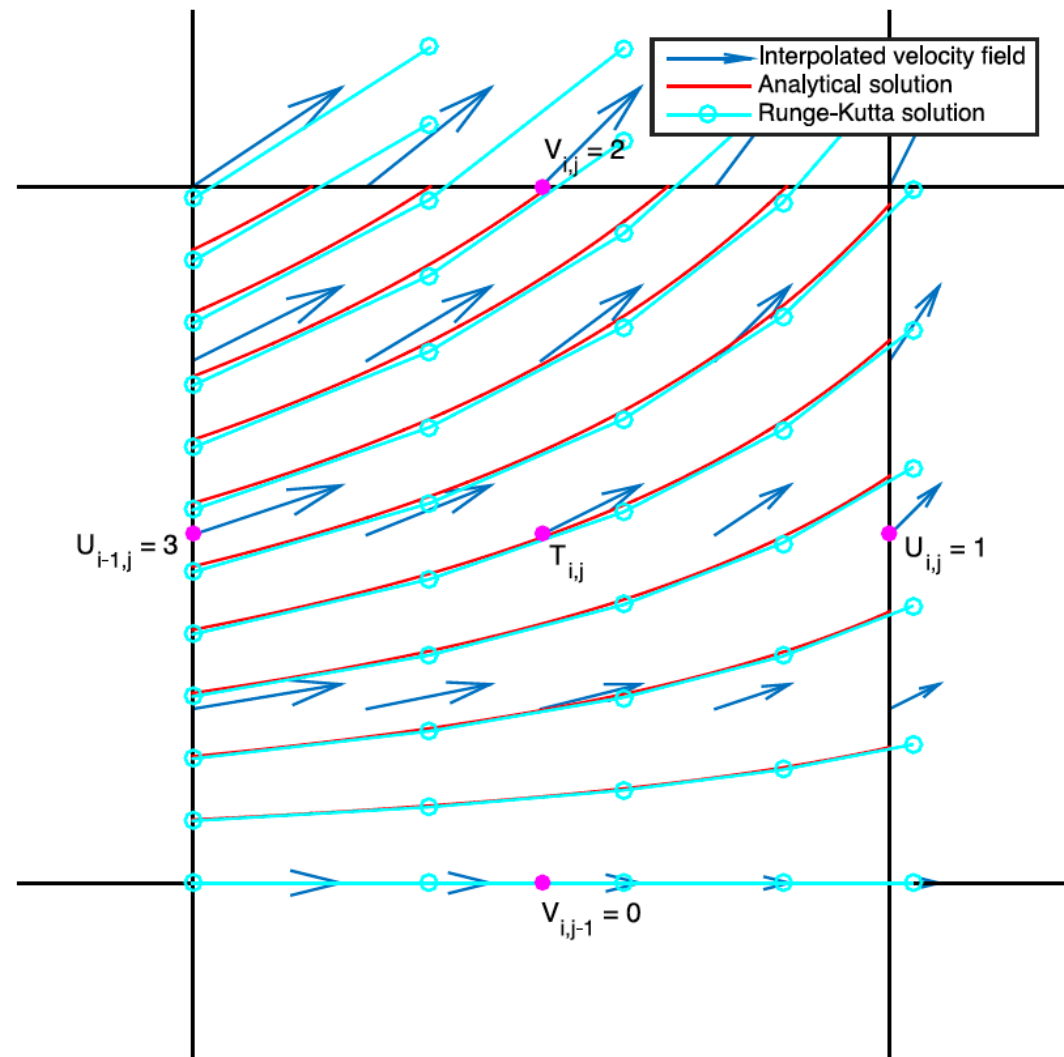


Fig. 2. Illustration of time stepping solutions on an Arakawa C-grid with edges of non-dimensional length = 1. Velocities (u , v) across the four edges are given in numbers at the magenta dots. The blue arrows are the linearly interpolated velocities within the grid. Assume particles are released on the $i - 1$ (left) edge. The red lines are pathlines of the analytical solution for these particles. The cyan piecewise linear lines are the solutions to RK4 timestepping with $dt = 0.1$. The two types of integration lead to similar solutions. (For interpretation of the references to colour in this figure legend, the reader is referred to the web version of this article.)

Stochastic trajectories using the Fokker-Planck Equation

$$dX_i(t) = a_i(t, \mathbf{X})dt + \sigma_{ik}(t, \mathbf{x})dW_k(t), \mathbf{X}(t_0) = \mathbf{X}_0$$

Deterministic drift

Diffusion operator

$$dX_i(t) = \left(v_i^\dagger + \frac{\partial K_{ij}}{\partial x_j} \right) dt + \sigma_{ik}(t, X) dW_k(t)$$

$$dX_i(t + \Delta t) = X_i(t) + \left(v_i^\dagger + \frac{\partial K_{ij}}{\partial x_j} \right) \Delta t + \sigma_{ik}(t, X) \Delta W_k(t)$$

3.3.2 Hierarchy of Markov Models: “Ad Hoc Method”

$$\mathbf{X}(t + \Delta t) = \mathbf{X}(t) + (1 + \epsilon) \int_t^{t+\Delta t} \mathbf{v}(\mathbf{x}, t) dt$$



$$\mathbf{X}(t + \Delta t) = \mathbf{X}(t) + \int_t^{t+\Delta t} [\mathbf{v}(\mathbf{x}, t) + \mathbf{v}_{\text{noise}}(\mathbf{x}, t)] dt$$

For divergent
free:

$$\mathbf{v}_{\text{noise}}(\mathbf{x}) = \nabla \times \psi_{\text{noise}}(\mathbf{x})$$

V_{noise} can be random walk as in $\mathbf{V}_{\text{noise}} = R\sqrt{2K\Delta t}$

With many other flavors of this parameterization ...

“It is also still open how the Fokker-Plank Equation approach (Section 3.3.1) and the ad-hoc Markov model approach (Section 3.3.2) can be combined. While the first approach is more mathematically rigorous, the second provides an insight into the properties of observed or simulated oceanic turbulence on different scales and in different regions, and may be useful in building future parameterizations of eddy induced transport in terms of Lagrangian stochastic parameterizations.”

Particle Diagnostics

Lagrangian Coherent Structures

$$FTLE(x_0, t_0, \tau) = \frac{1}{\tau} \ln \sqrt{\lambda_{max}}$$

λ = Eigenvalue of Cauchy Green Strain Tensor

SST Backward FSLE 2013-01-01 00:00

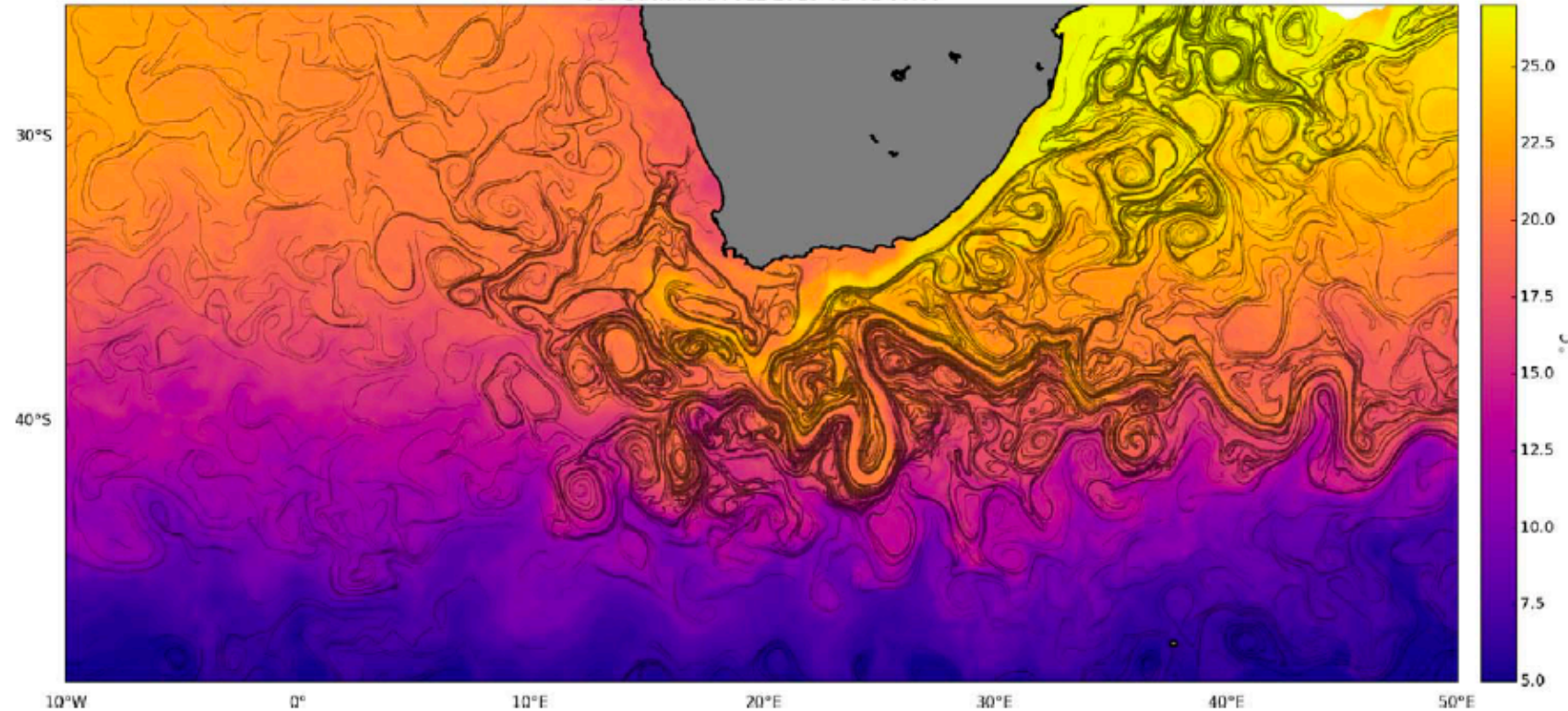
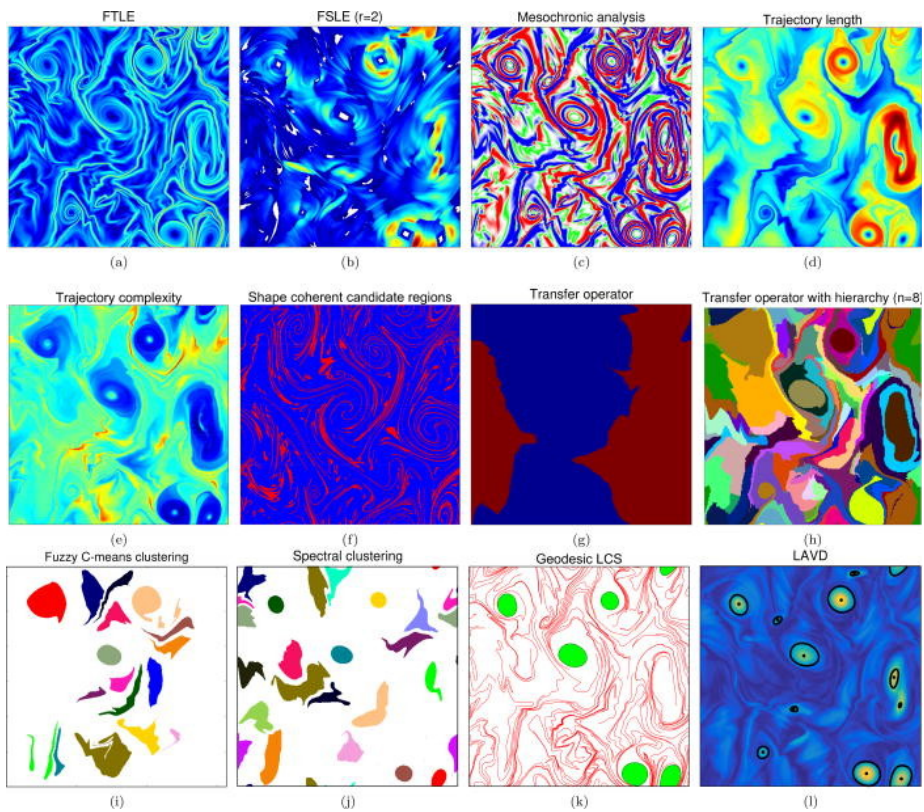


Fig. 3. Backward Finite Size Lyapunov Exponents for January 1 2013 computed as in d'Ovidio et al. (2004), with initial separation distance of 0.01° and final separation distance of 1° . The FSLE have been computed using surface absolute geostrophic velocities produced by Ssalto/Duacs and distributed by AVISO, with support from CNES (delayed time, all satellite merged product). Ridges of FSLE (≥ 0.3) are overlaid on Multi-scale Ultra-high Resolution (MUR) Sea Surface Temperature (<http://mur.jpl.nasa.gov/>), showing good correspondence between the Lagrangian coherent structures and the distribution of the surface tracer advected by the Agulhas current, the Agulhas retroflection and their associated mesoscale activity.



A. FTLE method

Strengths: Simple and objective algorithm; FTLE ridges capture hyperbolic LCSs under additional mathematical conditions (cf. Ref. 82); FTLE trenches tend to approximate jet cores (but see Ref. 27 for exceptions).

Weaknesses: No reliable detection of elliptic LCSs; ridges connect locations of high stretching with those of high shear, and hence also produce false positives for hyperbolic LCS.

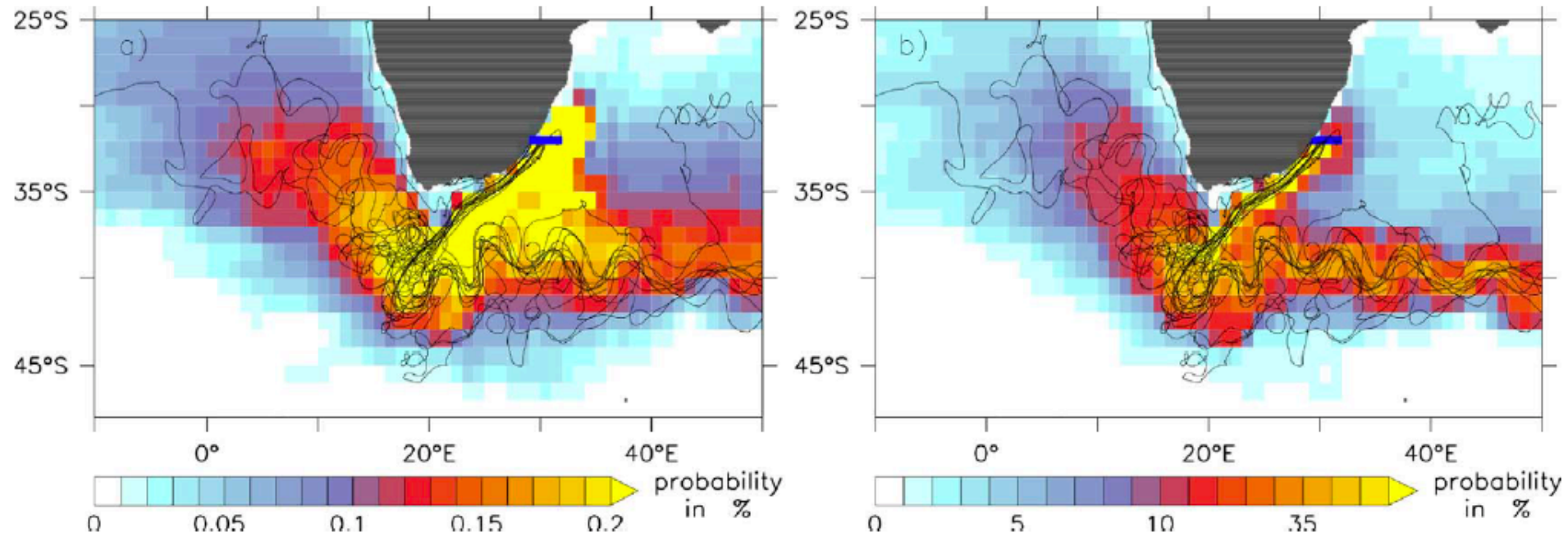


Fig. 4. Lagrangian modelling approach to determine pathways of particles released in the Agulhas Current at 32°S (blue line extending east from Southeast Africa), based on a set of 5-year long trajectories initialized in the year 2000 (some examples visualized as black lines): a) Probability with that a 1°x1° bin spanning the whole depth range is occupied by a particle during the considered time span. The probability for each bin has been obtained by counting the number of particles occupying this bin at each time step, summing up this particle counts over the whole integration period and then dividing it by the total number of recorded particle counts for all bins. Thus, the sum of the probabilities of all bins yields 100%; b) Probability that a particle occupies a particular bin at least once during the considered time span. In this case the probability for each bin has been obtained by counting the number of different particles occupying this bin and dividing by the total number of particles. Thus, the probability for each bin can range between 0 and 100%. The Lagrangian analysis was performed with the ARIANE tool using the 3D 5day-mean velocity fields from the high-resolution model INALT01 (Durgadoo et al., 2013). (For interpretation of the references to colour in this figure legend, the reader is referred to the web version of this article.)

Origin, dynamics and evolution of ocean garbage patches from observed surface drifters

Basic Idea

Erik van Sebille^{1,3}, Matthew H England¹ and Gary Froyland²

¹ Climate Change Research Centre and ARC Centre of Excellence for Climate System Science, University of New South Wales, Sydney, Australia

² School of Mathematics and Statistics, University of New South Wales, Sydney, Australia

- Use floats to predict where particles will go without models. Dynamics are baked in!
- Evolution of the concentration vector can be described by the naive Markov Matrix

SÉVELLEC ET AL.

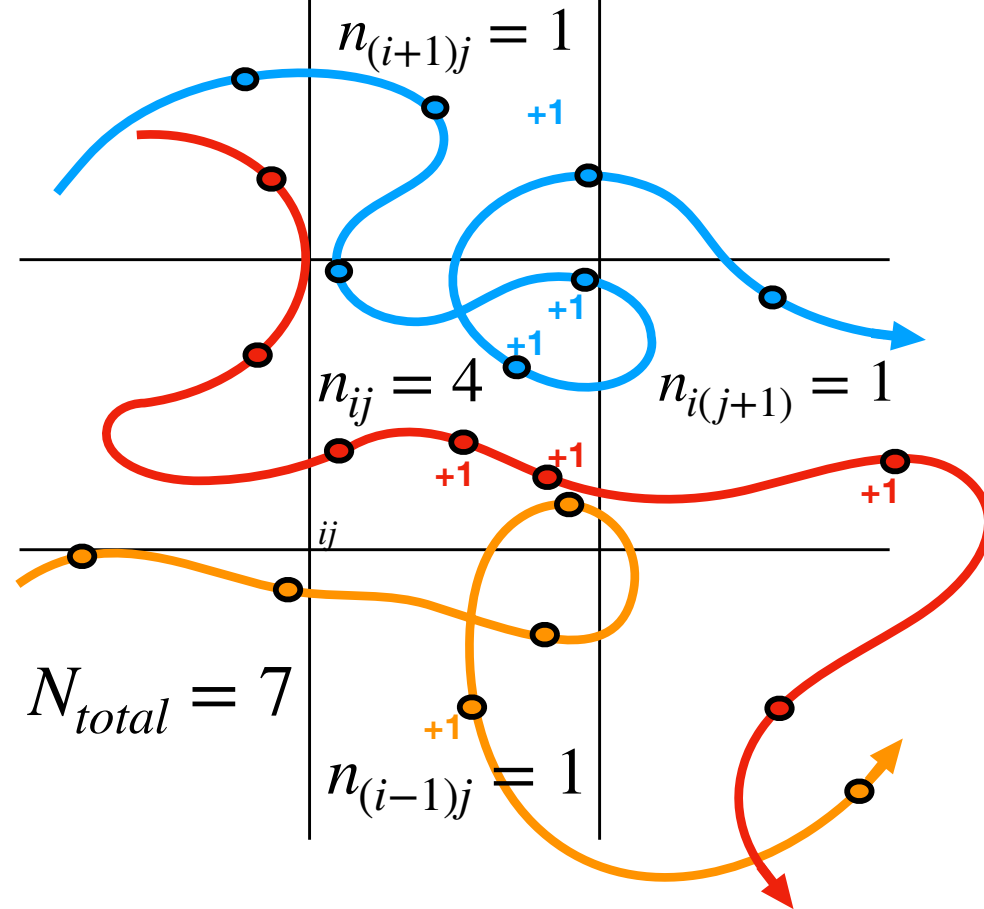
$$\rho(t + \tau) = \mathbf{H}(\tau)\rho(t), \quad \text{where} \quad \mathbf{H}(\tau) = \mathbf{M}^k \quad (4)$$

McAdam and Sebille 2018

Sevellec et al. 2017

Maximenko 2012

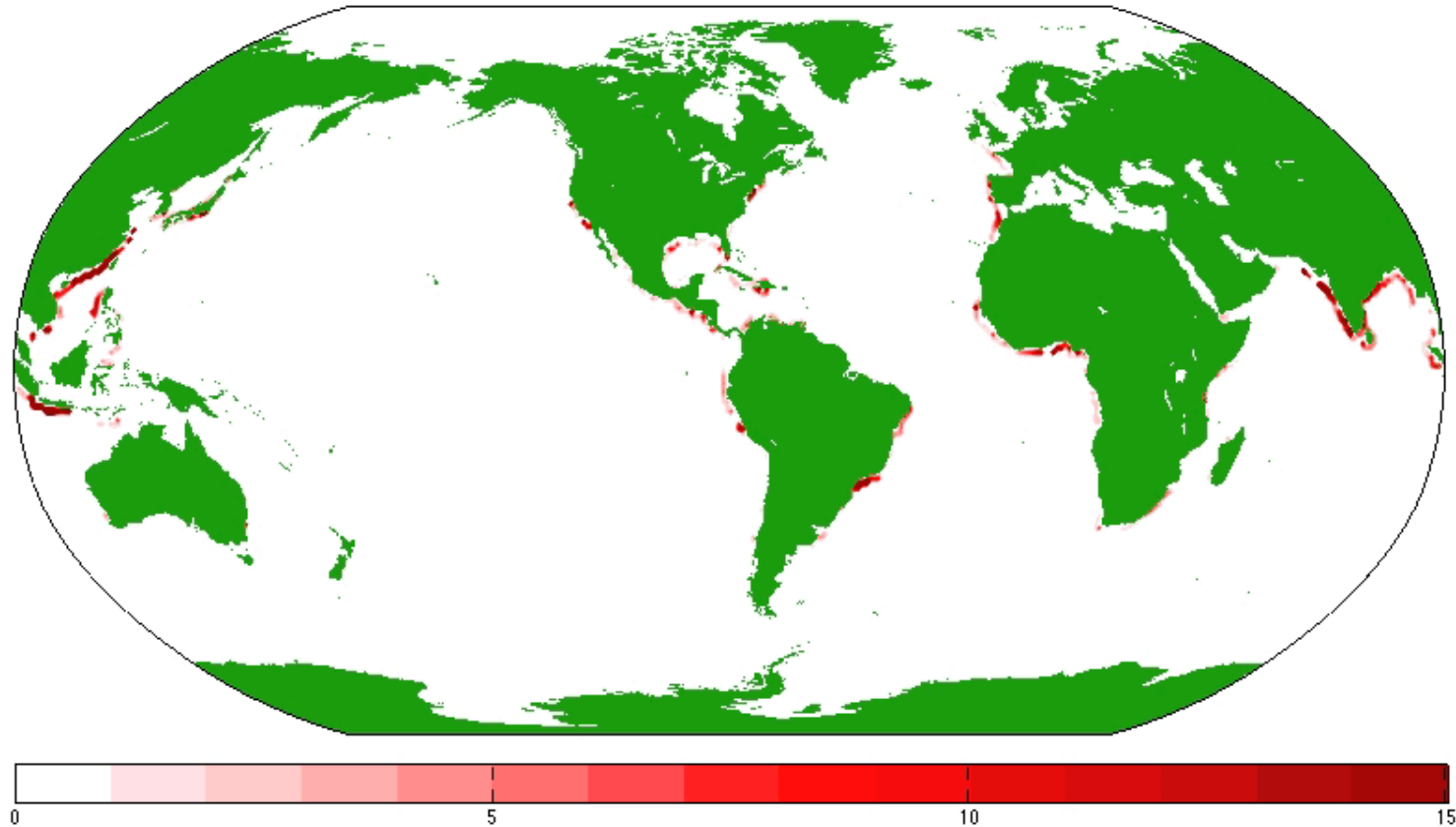
Basic Idea



Courtesy of Erik Van Sebille

Surface Drift - Where do Coastal Plastics Go? (Based on surface drifter measurements)

Tracer accumulation factor 0 years and 00 months after release



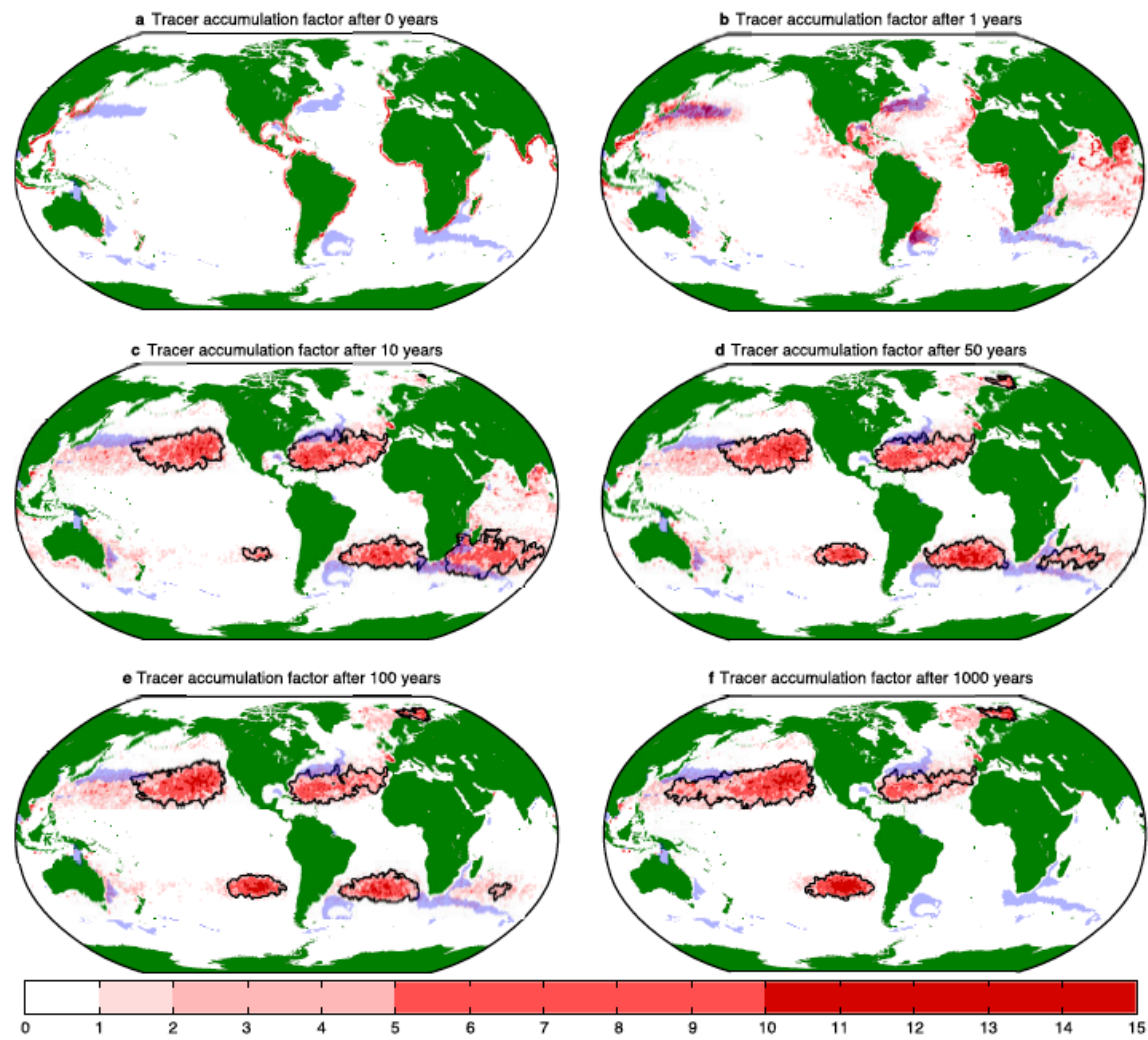


Figure 1. The locations and sources of the six garbage patches. (a) The tracer accumulation factor (TAF) at the moment of release. Coastal population is used as a proxy for the amount of tracer released. The blue patches denote areas where sea surface height variability is larger than 15 cm, an indication of high eddy activity. Note that in these figures, as well as in the video in the supplementary material (available at stacks.iop.org/ERL/7/044040/mmedia), white shading means that the tracer accumulation factor (TAF, see also section 2) is less than 1. (b) The TAF after 1 yr of integrating the tracer. The tracer is advected into the open ocean by the swift-flowing surface currents. (c) The TAF after 10 yr of integrating the tracer. Well-defined patches can be seen in each of the five subtropical gyres. The thick lines denote the spatial extent of the patches. (d) The TAF after 50 yr of integrating the tracer. The Southern Indian patch has become much smaller, while the Southern Pacific one has grown considerably in comparison to the tracer density after 10 yr. A sixth patch is now visible in the Barents Sea. (e) The TAF after 100 yr of integrating the tracer. The patch in the South Indian has almost completely disappeared. (f) The TAF after 1000 yr of integrating the tracer. The patches in the Southern Atlantic and Indian have completely disappeared, and the patches in the South and North Pacific have grown considerably in size.



You are welcome and free to use the data in the file above for your scientific work. I just ask that you cite this scientific article in any publications that use the data. Both the data and the paper are licensed under a Creative Commons Attribution-NonCommercial-ShareAlike license. Map tiles by Stamen Design, under CC BY 3.0. Data by OpenStreetMap, under CC BY SA. If you have any questions

Imperial College London

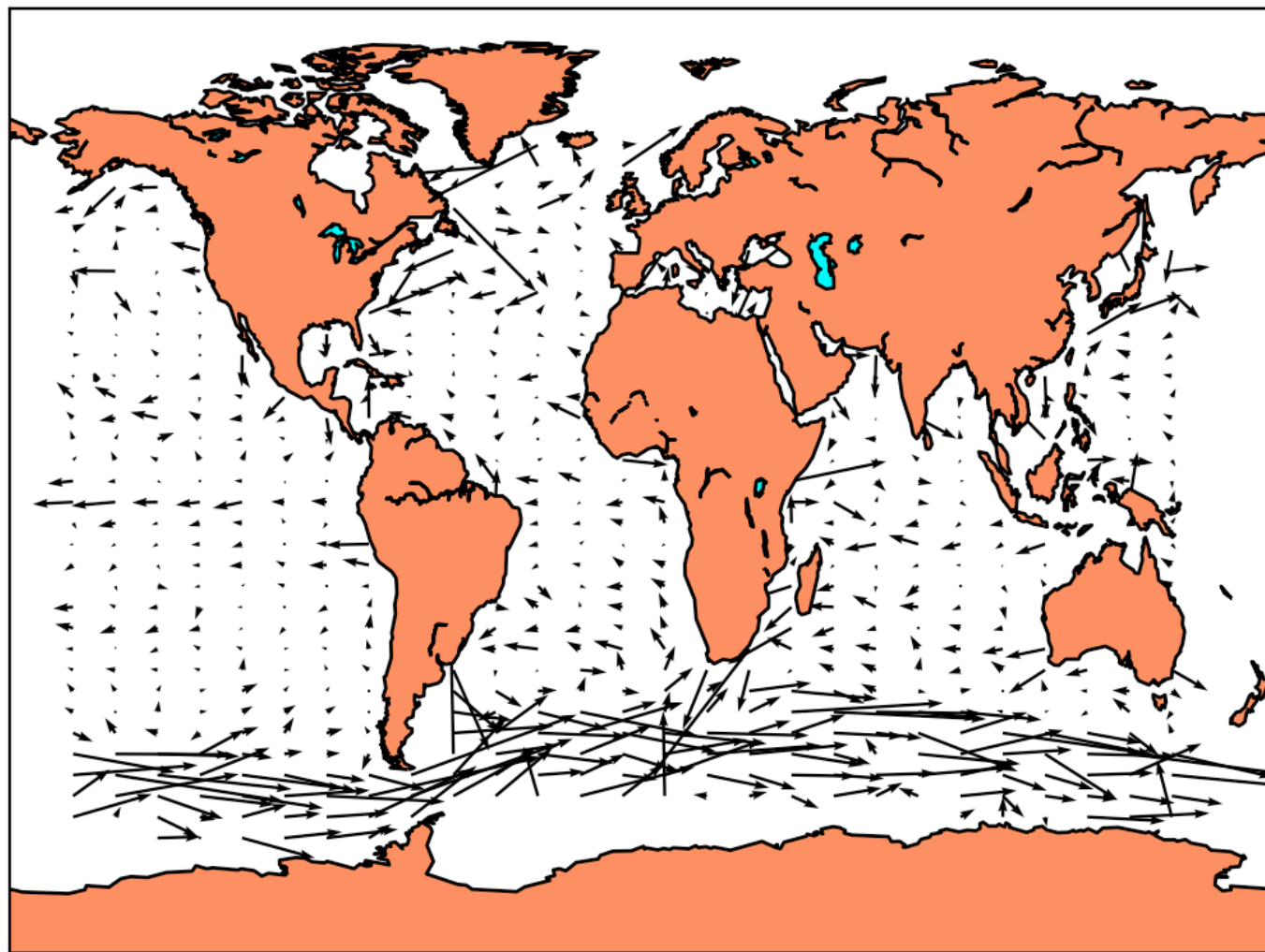
Grantham Institute
Centre for Environmental Change and the Environment

Data Science Institute

ARC CENTRE OF EXCELLENCE FOR CLIMATE SYSTEM SCIENCE

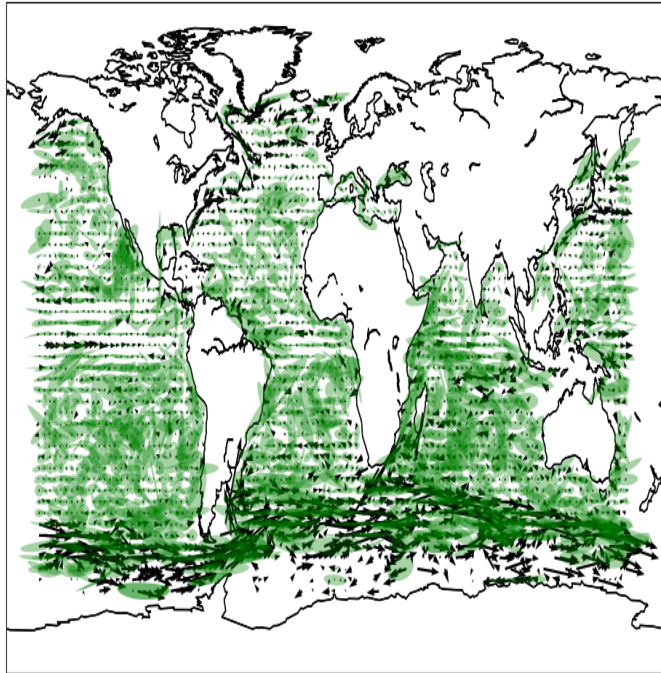


Mean Transition

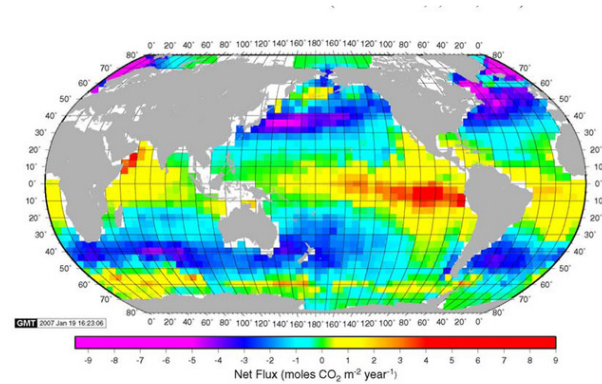


Network Design

Variance Ellipses of Transition Matrix



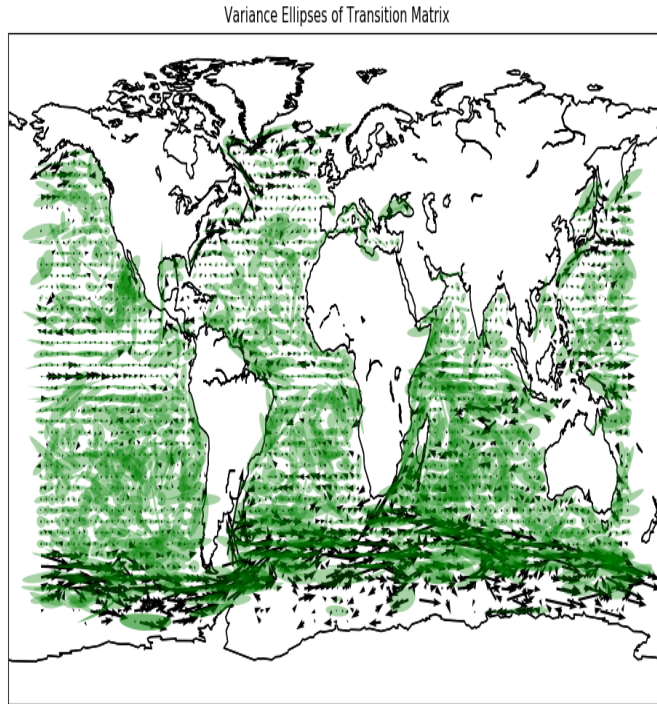
BGCArgo Network =



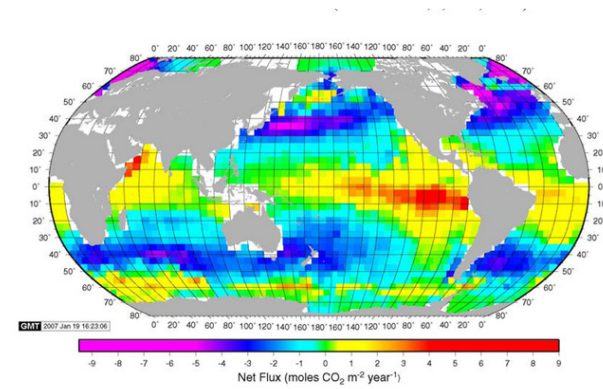
Takahashi et al.

Network Design

BGC Argo Network =



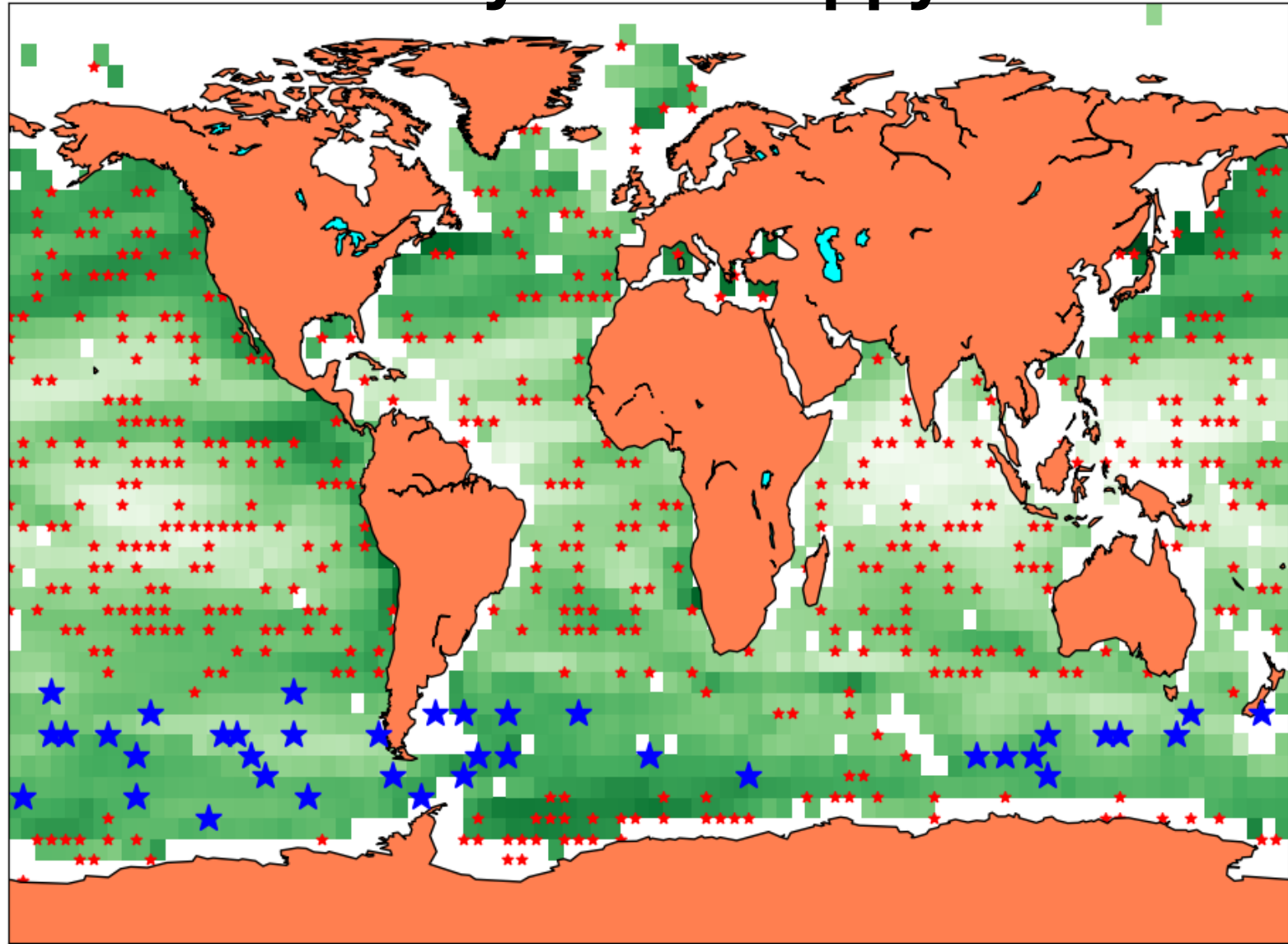
-1



Takahashi et al.

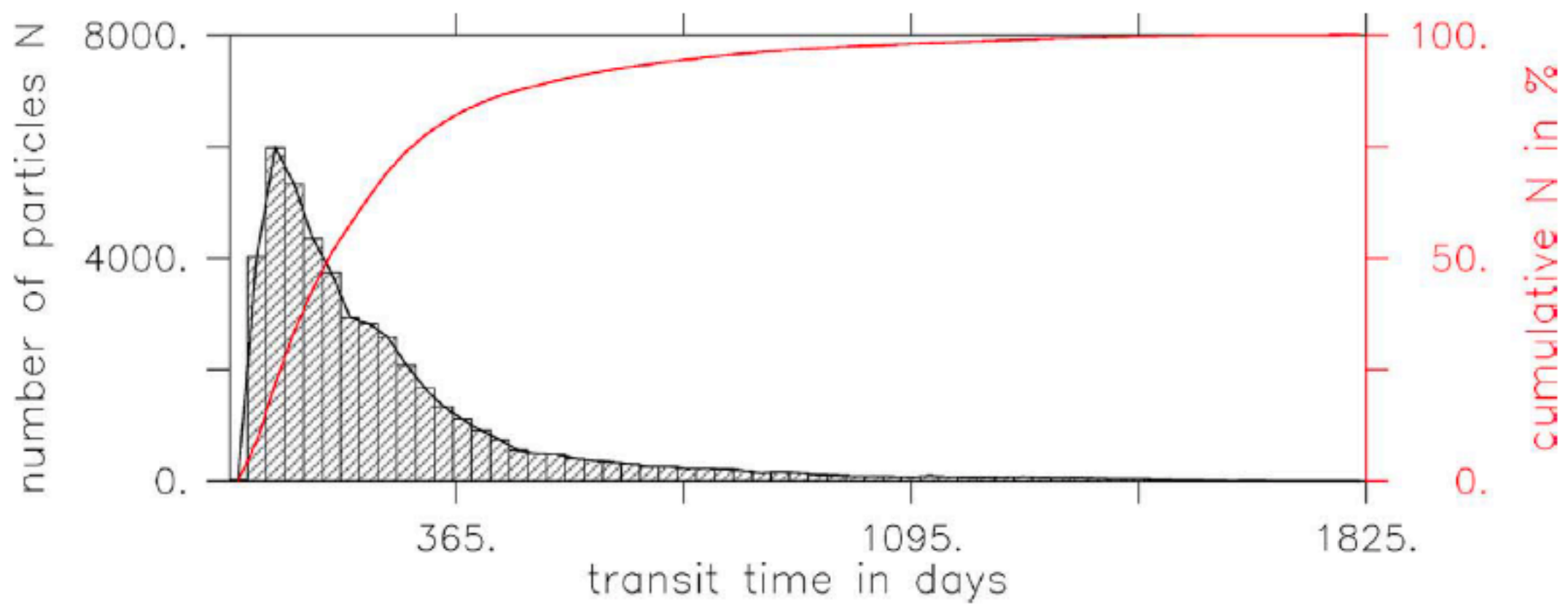
Everyone is happy!

$\rho_0(t) =$



Summary:

- Lagrangian analysis can be a powerful tool for answering questions regarding pathways and tracer exchange
- Transport tensor can be difficult to define rigorously
- In practice stochastic terms may be added to estimate unresolved model physics
- Markov matrices (transition matrices) offer naive estimates for particle PDFs and can be used for optimal network design



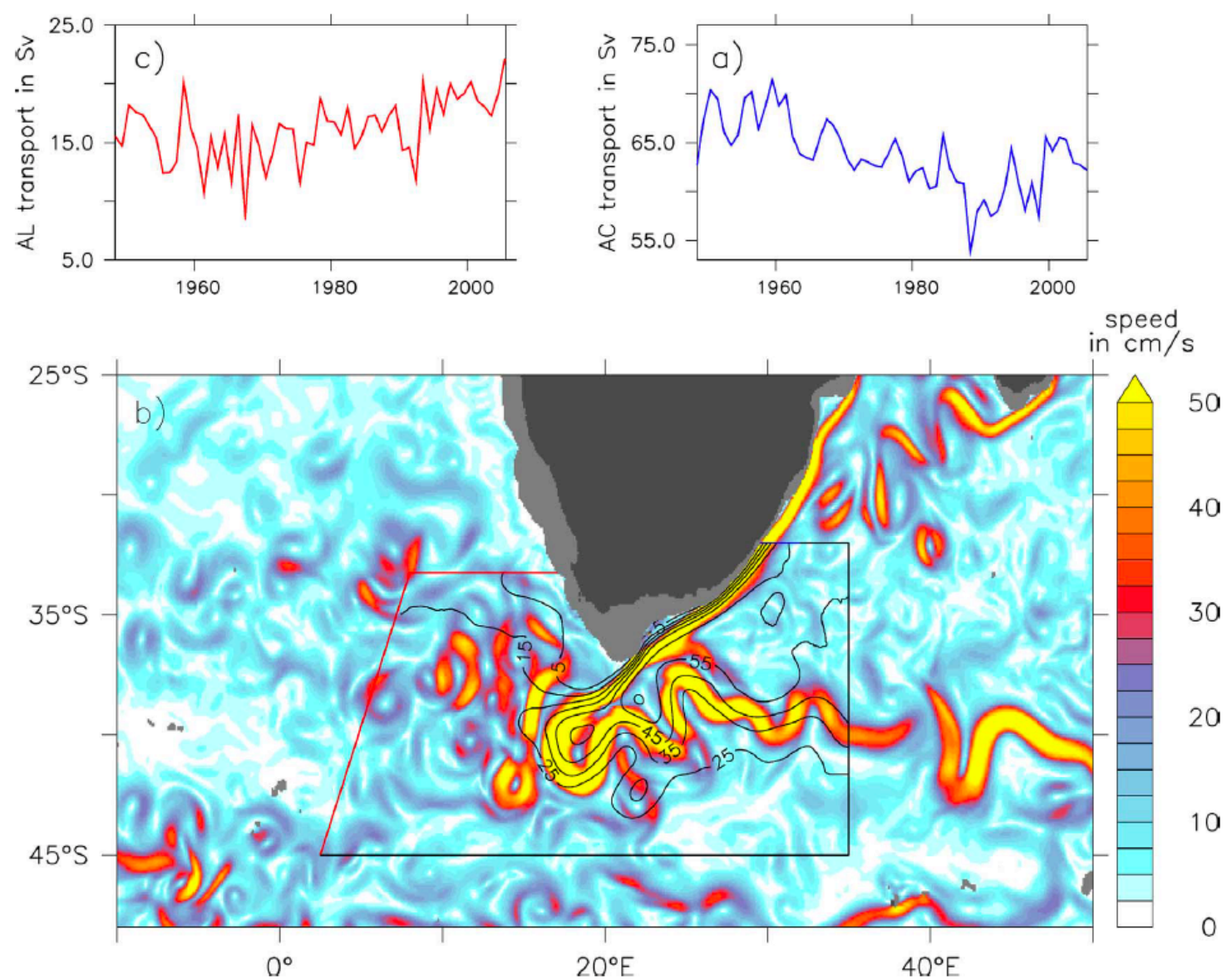


Fig. 6. Quantitative Lagrangian modelling approach to determine Agulhas Leakage: a) Time series of the annual Agulhas Current (AC) transport at 32°S, where particles were released continuously proportional to the current volume transport, each particle associated with a fraction of this transport; b) Snapshot (18-Apr-2000) of current speed at 450 m depth in the Agulhas region (colour shading, in cm/s), as well as the horizontal Lagrangian streamfunction (contours, in Sv) for all trajectories initialized in the year 2000 and traced along 3D streamlines towards the control sections (black and red lines); c) Time series of annual Agulhas Leakage (AL) transport, obtained by considering for each release year only the transports of those trajectories, that cross the approximated GoodHope section (red lines) within 5 years. The Lagrangian analysis was performed with the ARIANE tool using the 3D 5day-mean velocity fields from the high-resolution model INALT01 (Durgadoo et al., 2013). (For interpretation of the references to colour in this figure legend, the reader is referred to the web version of this article.)

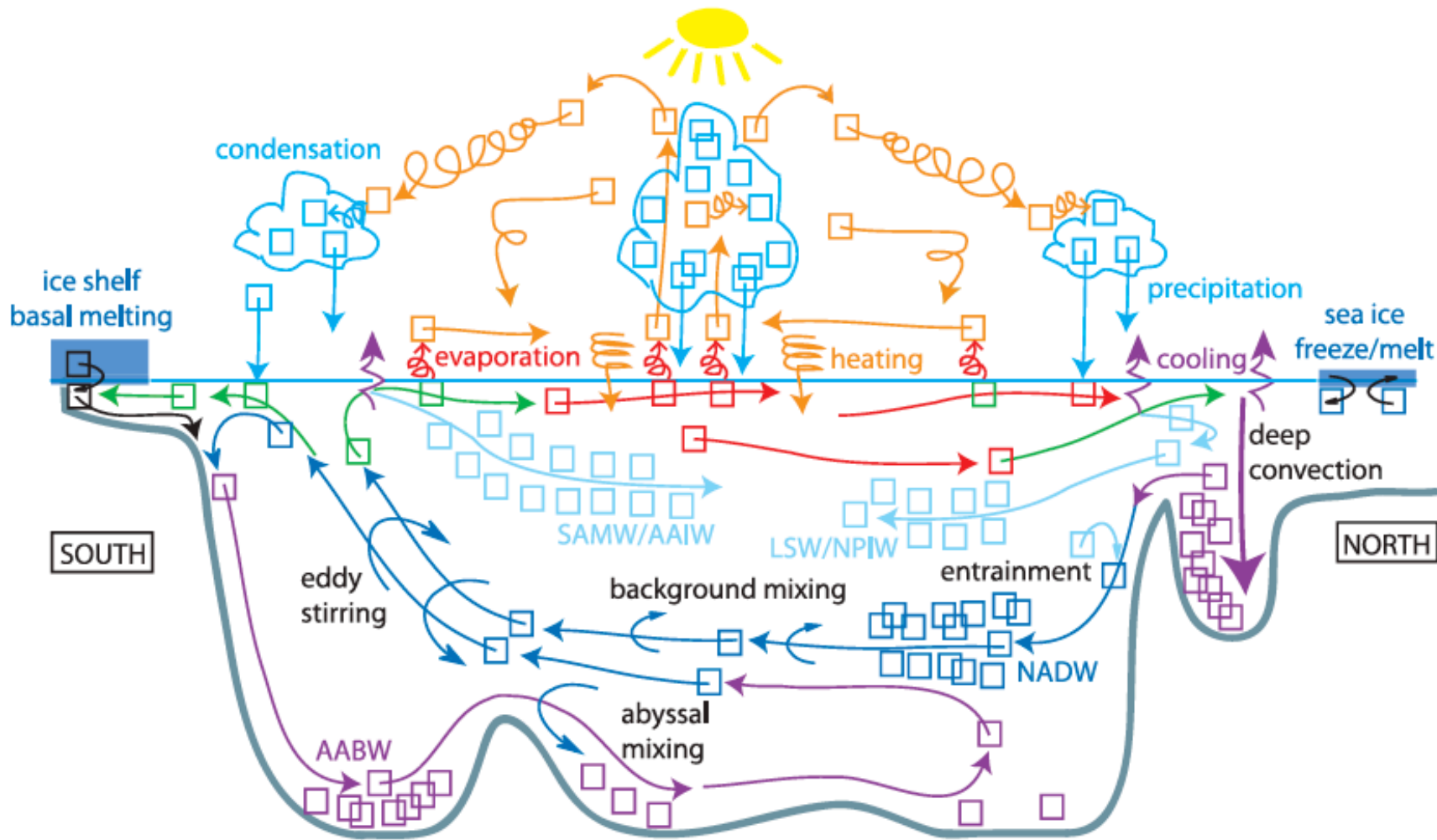


Fig. 7. Illustrating how water particles follow the water cycle in the Earth System. We emphasize here the global ocean conveyor circulation in a pole-to-pole, meridional-vertical plane, coupled to selected and idealized atmospheric circulation in the same plane, omitting land for convenience [terrestrial processes such as evapo-transpiration, storage and runoff are also part of the full water cycle]. Individual water particles are represented by color-coded boxes, advected quickly/chaotically through the atmosphere, and slowly/steadily through the ocean. Particles are stored on a wide range of time-scales: in clouds (hours–days); in sea ice (seasons–years); in the ocean (years–centuries); in ice sheets/shelves (centuries–millennia). In the ocean, colour coding identifies selected water masses and advection thereof: Antarctic Bottom Water (AABW); North Atlantic Deep Water (NADW); Labrador Sea Water (LSW); Antarctic Intermediate Water (AAIW); North Pacific Intermediate Water (NPIW); Subantarctic Mode Water (SAMW). In the atmosphere, colour-coding distinguishes vapour and liquid phases. Highlighted processes involve phase change or ocean-atmosphere exchange: ocean surface heating/cooling; evaporation; condensation; precipitation; sea ice freezing/melting; ice shelf basal melting.

Highlighted processes internal to the ocean transform water particle density: deep convection; entrainment; enhanced abyssal mixing; eddy stirring; weak background mixing. (For interpretation of the references to colour in this figure legend, the reader is referred to the web version of this article.)

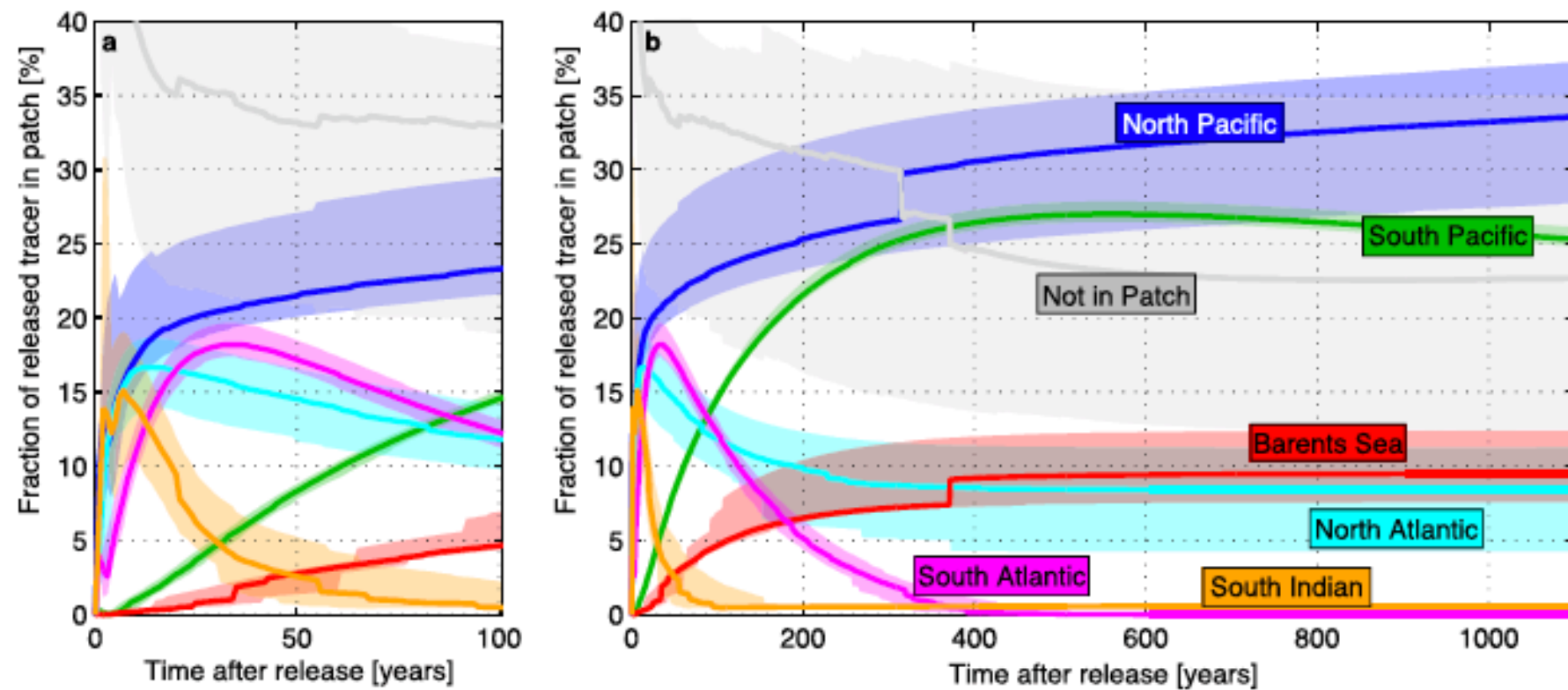


Figure 2. The evolution of the amount of tracer within the six garbage patches. For each of the six garbage patches, the amount of tracer in the area where the $TAF > 2.0$ (thick lines, see also figure 1) as a function of time for (a) the first 100 yr after release and (b) the first 1100 yr. The shaded areas depict the sensitivity to the choice of TAF value, here shown as the range $1.0 < TAF < 3.0$. Near instantaneous jumps in the patch size are due to mergers of patches and depend on the exact value of the TAF criterion used. The North Pacific patch keeps on growing for at least 1100 yr after the release of tracer, while the South Pacific patch slowly decays after reaching a maximum size at 500 yr. The North Atlantic and Barents Sea patches reach an equilibrium size after approximately 300 yr, while the South Atlantic and South Indian patches completely disperse within 400 and 100 yr, respectively. The amount of tracer not within any of the six main patches stabilizes at approximately 22% of total tracer released. Part of this tracer not in patches accumulates in small localized areas such as the Bay of Biscay (figure 1(d)), but most of it (13% of the total tracer released) resides on the fringes of the patches, where the $TAF < 2.0$. Note that in this model, tracer is released only in the first year, and that by construction tracer is conserved, meaning no export onto the coasts or into the deep ocean.

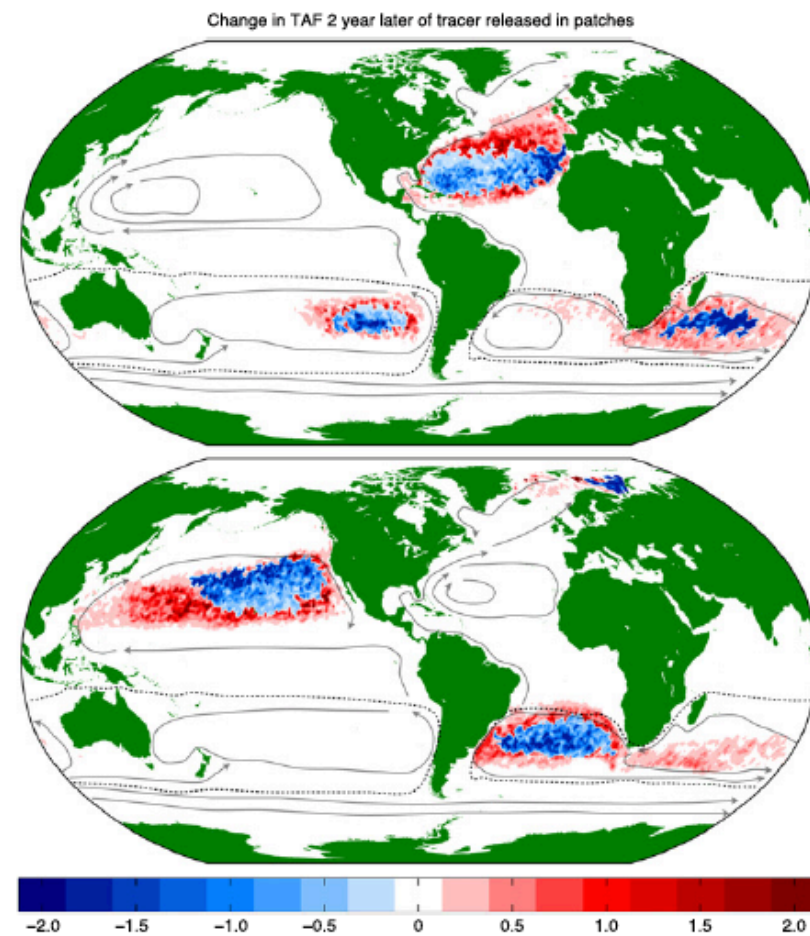
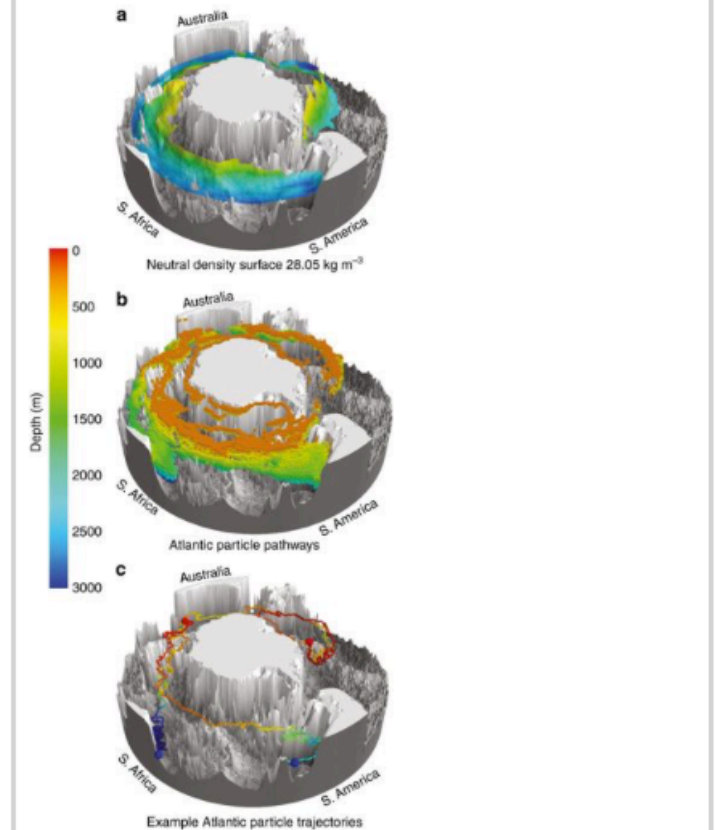


Figure 3. The spatial pattern of leakiness for the six garbage patches. For each of the six garbage patches tracer is released only within the patch at its simulated concentration after 50 yr (the black contours in figure 1(d)). That tracer is then integrated for another 2 yr, and this figure shows the increase (red) or decrease (blue) in TAF after this 2 yr period. There are two separate maps shown in order to disentangle the different patches, in particular the South Atlantic and South Indian ones. Whereas the tracer that leaves the two Pacific patches does so rather isotropically, the leakage of the other four patches clearly has a preferred direction. The grey flow arrows depict the major ocean currents and pathways, with the dashed line encompassing the Southern Hemisphere super-gyre (Speich *et al* 2007).

“Using Lagrangian particles to temporally resolve for example the meridional overturning circulation (Blanke et al., 1999; Thomas et al., 2015b) or inter-basin connectivity (Blanke and Speich, 2002) can be difficult with many state of the art climate models. To address this problem, a commonly employed ad hoc method is to loop the model data in time such that the velocity and tracer fields are returned to the first time step once the end has been reached (e.g., Döös et al., 2008; van Sebille et al., 2012; Thomas et al., 2015b). This approach thus permits particles to be advected for longer time scales than available from the raw data. However, particle looping can only work if the model has no drift in the velocity or tracer fields, that there are no large unphysical jumps in the fields between the end and the beginning of the model run, and that any unphysical jumps will have a small net effect on the particle pathways.”

Fig. 1



The three dimensional upward spiral of North Atlantic Deep Water through the Southern Ocean. **a** Observed warm water (>1.6 °C) on the 28.05 kg m⁻³ neutral density surface from hydrographic observations²⁷, south of 40° S, colored by depth (m). The isoneutral surface is masked in regions with potential temperature below 1.6 °C. 1/4° ocean bathymetry⁷⁰ is shown in gray. **b** Modeled (CM2.6) particle pathways from the Atlantic Ocean, with particles released in the depth range 1000–3500 m along 30° S. Colored boxes mark 1° latitude × 1° longitude × 100 m depth grid boxes visited by >3.5% of the total upwelling particle-transport from release at 30° S to the mixed layer. Boxes are colored by depth, similar to **a**. **c** Two example upwelling particle trajectories from CM2.6, one originating from the western Atlantic and the other from the eastern Atlantic. Trajectories are colored by depth as in **a** and **b**, blue spheres show the particle release locations and red spheres show the location where the particles reach the mixed layer. Three-dimensional maps were produced using Python and Mayavi⁷¹